

Static Hot-Fire Testing of a Green Hybrid Rocket Engine

Mohamed Tarmizi Ahmad ^{1*}, Anudiipnath Jagannathan ¹, Razali Abidin ¹,
Amzari Zhahir ^{2**}, Muhammad Nur Farhan Saniman ³

¹*Centre of Defence Research and Technology, National Defence University of Malaysia,
Kem Sungai Besi, 57000 Kuala Lumpur, Malaysia*

²*Department of Aerospace Engineering, Faculty of Engineering, Universiti Putra Malaysia,
43400 UPM Serdang, Selangor, Malaysia*

³*Mechanical Engineering Section, Universiti Kuala Lumpur – Malaysia France Institute,
43650 Bandar Baru Bangi, Selangor, Malaysia*

ABSTRACT

This paper presents the conduct of the hot-fire testing for a green hybrid rocket engine. The hybrid rocket engine consists of liquid nitrous oxide (N₂O) as the oxidizer, with the stearic acid as the solid fuel and the incorporation of carbon nanotube and aluminum powder as the additives. From the conducted experimental, all systems that have been designed and developed in this study for the green hybrid rocket engine are demonstrated to be successful and fully functional, which also include the radio frequency control unit. Based on the results of the experiment, the developed laboratory-scale green hybrid rocket motor has been successfully ignited and produced a maximum thrust of 348 N, with the maximum combustion chamber pressure is recorded as 14 bar. In addition, several suggestions to improve the hybrid rocket engine design are also discussed.

Keywords: Oxidizer flow control, Nitrous oxide, Green hybrid rocket engine, Static hybrid rocket, Stearic acid fuel

I. INTRODUCTION

The traditional hybrid rockets, which have numerous advantages over their pure solid or liquid equivalents, are composed of solid fuel grains and a fluidic oxidizer [1]. In general, they are especially safer to create, store and ship. Additionally, they can provide higher specific impulse and density specific impulse, smooth thrust transition and also better controllability due to their start-and-stop capabilities in comparison to some of the solid and liquid propellants [2]. Moreover, the hybrid rockets can use denser fuels than liquid propellant systems and are mechanically simpler to run. However, hybrid rockets also have some drawbacks including pressure instabilities, relatively low combustion efficiency, inevitable fuel leftovers and fluctuations in the mixture ratio during operation [3,4]. In conjunction to this, the solid fuel regression rate is a common measure of the

performance of hybrid rocket, which also becomes the key factor that determines the design of the hybrid fuel grains and consequently the overall design of a hybrid motor [5].

Several studies and discussions have been published on the principal theories of how the solid hybrid fuel burns, which among others also include [6-8]. In short, the following explanation is based the research works in [9-11] that involve in-depth fundamental studies on hybrid combustion. Based on the research work, the hypothesis is based on the turbulent diffusion flame model. This notion states that in a hybrid motor, combustion usually occurs in the boundary layer above the surface of the fuel rather than directly at the surface. The boundary layer is supposed to be turbulent since the hybrid motors have a high injection Reynolds number. According to the combustion model, the boundary layer will have two zones: one is above the flame where the temperature and velocity gradients are opposed

Manuscript received, November 19, 2023, final revision, December 7, 2023

* To whom correspondence should be addressed, E-mail: m.tarmizi@upnm.edu.my

** To whom correspondence should be addressed, E-mail: amzari@upm.edu.my

in direction and another one is below the flame where the gradients are in the same direction [12]. The depiction of these two zones is shown in Figure 1. Both zones together form the boundary layer for momentum transfer. Upon

ignition, a diffusion flame area will form within this boundary layer. The flame's convection and also radiation will then heat up the fuel surface.

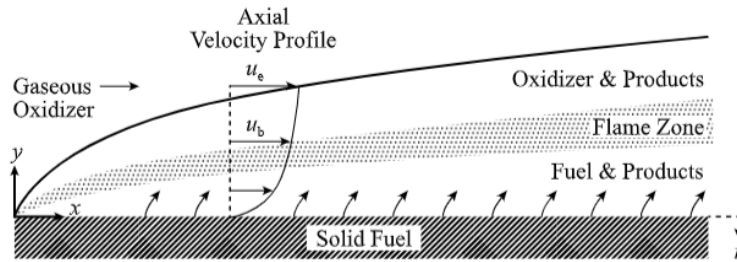


Figure 1 Diffusion combustion process in hybrid rockets [12]

By its very nature, liquid nitrous oxide offers several advantages as an oxidizer for the hybrid rocket engines. It is stable and generally unreactive at ordinary temperatures, which means it can be easily stored at room temperatures [13]. In addition, it is inexpensive, simple to use, non-toxic, environmental-friendly and self-pressurizing [14]. On the other hand, it also has the drawback of making the motor system heavier because the required ideal oxidizer-to-fuel ratio is higher than other common oxidizers [14]. Recently, there have been high interest for green propellants as well due to greater environmental awareness of the public [15]. In view of this, stearic acid is a potential solid propellant due to its similarity to kerosene, which many experts think has potential as a fuel for hybrid rockets [16]. It should be noted that stearic acid is a "green" propellant that is widely accessible, sustainable and produced as a byproduct of the production of palm oil. Companies that produce palm oil also produce the majority of the stearic acid, which means that it is easily available locally in Malaysia. However, since the melting temperature was low 69.3°C most of the melted wax was expelled from the nozzle [17]. To prevent this phenomenon, carbon nanotube (CNT) was added and to compensate for reduced regression rate aluminum powder was added. Based on Bomb Calorimeter test 3% CNT and 27% Al provides higher calorific values of 10538 Cal/g [18].

In this study, a green hybrid rocket engine is analyzed in a hot-fire experimental testing. The hybrid rocket engine is constructed with liquid nitrous oxide as the oxidizer and stearic acid doped with CNT and Al as the solid propellant. Based on the obtained results, the performance of the hybrid rocket motor can be established.

1.1 Fuel Regression

Fuel regression is the rate at which the solid fuel being burnt over time. There are several theories and test being conducted since the 1930's to investigate the potential the regression in hybrid rocket motor. The combustion process in hybrid rocket motor is far more complicated than a solid rocket because in hybrid, as the solid fuel being burnt, both the shape and mass flux will change. Thus, this will affect the fuel regression and all the thermodynamics properties of the combustion products as well as the oxidizer to fuel ratio (O/F).

In the early time, there was a formula develop to calculate the fuel regression in solid rockets and for that formula being used in the hybrids is not very practical because of accuracy. The St. Robert's law [19]. Several studies have demonstrated that hybrid fuel regression rates have little or no dependence on chamber pressure [20].

$$\dot{r} = aP_0^n \quad (1)$$

Marxman and Gilbert first proposed an enthalpy-based fuel regression model for hybrid rocket motors in the early 1960's [21]. The fundamental assumption made by Marxman and his colleagues was that regression rates in a hybrid rocket are dominated by thermal diffusion and not chemical kinetics [22]. However, in a hybrid rockets, regression is mainly a function of turbulent boundary layer heat transfer. Oxidizer flowing from the center will be mixed with the floating vapors from solid fuels when boundary layer is created. The heat transfer from the inner part of the solid fuel wall region will drive the regression rate. The inner part is where the combustion process between the oxidizer and solid fuel take place.

The relations between the regression and heat flux are proportional and can be write as:

$$\rho_f \dot{r} = \frac{\dot{Q}_w}{\Delta H} \quad (2)$$

The regression rate in a turbulent boundary layer can be parameterized in the terms of Stanton number and mass flux as:

$$\dot{r} = \frac{0.03GRe_z^{-0.2}}{\rho_f} \frac{C_H}{C_{H0}} \frac{\mu_e}{\mu_c} \frac{(h_{cs} - h_{wg})}{\Delta H} \quad (3)$$

This shows that the radiation heat transfer is being neglected and this is a suitable assumption for most non-metal fuels. The Stanton number can also be categorized in terms of mass addition or blowing parameter as:

$$\frac{C_H}{C_{H0}} = 1.2B^{-0.77} \quad (4)$$

where,

$$B = \frac{\mu_e (h_{cs} - h_{wg})}{\mu_c \Delta H} \quad (5)$$

The simplified regression formula is created from the combination at the equations above and given as:

$$\dot{r} = 0.036 \frac{G}{\rho_f} Re_x^{-0.2} \left(\frac{\mu_e (h_{cs} - h_{wg})}{\mu_c \Delta H} \right)^{0.23} \quad (6)$$

Marxman and Muzzy later determined that regression rate is limited by the heat and mass transfer to the fuel surface [23]. This proved that as $h_{cs} - h_{wg}$ increase, \dot{r} also increase which indirectly support the blowing parameter which reduces \dot{r} . Up to this point, we can say that the regression rate is dependent on mass flux rather than changes in enthalpy. A further study done by Strand et al. [24] and later Chiaverini et al. [22] tells us that experimental coefficients predicted by Marxman were different from the theoretical values derived in the classical relation especially the exponents on mass flux and the surface blowing coefficient. Therefore, because of these derivations, Marxman original form of the model is rarely being used in modern hybrid rocket analysis. Additionally, the Marxman model relates the fuel regression rate to the surface skin friction, but does not close sufficiently to allow a prior regression rate prediction [25].

A closed form regression rate model based on flat plate flow theory was developed by Eilers and Whitmore [26] and corrected by Whitmore and Chandler [27] for non unity Prandtl number.

$$\dot{r} = \frac{0.047}{Pr^{0.153} \rho_{fuel}} \left(\frac{c_p [T_0 - T_{fuel}]}{h_{v fuel}} \right)^{0.23} \left[\frac{\dot{m}_{ox}}{A_{chamber}} \right]^{\frac{4}{5}} \left(\frac{\mu}{L} \right)^{\frac{1}{5}} \quad (7)$$

The parameters μ and Pr in the equation above are from the propellant gas properties. c_p , ρ_{fuel} , T_{fuel} and $h_{v fuel}$ refer to the properties of the solid fuel. $A_{chamber}$ and L are the fuel port cross sectional area and length of the solid fuel. It was used to predict regression along the length of hybrid rocket motor. It originates from the enthalpy balance between the latent heat of the burning fuel and heat convection into the combustion flame zone. By applying the generalized form of the Reynold's

$$\frac{\delta P_0}{\delta t} = \frac{A_{burn} \dot{r}}{V_c} [\rho_{fuel} R_g T_0 - P_0] - P_0 \left[\frac{A^*}{V_c} \sqrt{\gamma R_g T_0 \left(\frac{2}{\gamma+1} \right)^{\frac{\gamma+1}{\gamma-1}}} \right] + \frac{R_g T_0}{V_c} \dot{m}_{ox} \quad (12)$$

In the hybrid rocket motor, we can learn that fuel is being dumped in the core oxidizer flow. Thus, this blocks the channel flow from being fully develop until the region near fuel port. Figure 2 below shows the boundary layer growth process.

analogy between the Stanton number and the surface skin friction coefficient allows the heat transfer coefficient to be calculated. The model uses the Reynold's-Colburn analogy to relate the heat transfer at the surface of the fuel grain to the local boundary layer heat transfer, and overcomes the shortcoming of Marxman's original model.

In the equation above, the oxidizer mass flow rate of N_2O is modeled by the incompressible discharge coefficient formula:

$$\dot{m}_{ox} = C_d A_{ox} \sqrt{\frac{2\gamma}{\gamma-1} \rho_{ox} P_{ox} \left[\left(\frac{P_0}{P_{ox}} \right)^{\frac{2}{\gamma}} - \left(\frac{P_0}{P_{ox}} \right)^{\frac{\gamma+1}{\gamma}} \right]} \quad (8)$$

From Equation (7) we can see that that mean oxidizer mass flux through the port is in the third term in Equation (7) where it is known as G:

$$G = \frac{\dot{m}_{ox}}{A_{chamber}} \quad (9)$$

This supports the Marxman's idea where oxidizer mass flux is a huge factor in hybrid fuel grain regression rates. The total mass flow rate can be calculated by:

$$\dot{m}_{fuel} = A_{burn} \rho_{fuel} \dot{r} \quad (10)$$

From the above equation, we learn that total fuel port surface area is known as A_{burn} . We can then find the oxidizer to fuel ratio by:

$$\frac{O}{F} = \frac{\dot{m}_{ox}}{\dot{m}_{fuel}} = \frac{A_{ox} C_d \rho_{ox} \sqrt{2 \rho_{ox} (P_{ox} - P_0)}}{A_{burn} \rho_{fuel} \dot{r}} \quad (11)$$

Thus, from Equation (7) and Equation (11) we can learn that the P/F ratio will change accordingly with the burnt of fuel grain as the surface area changed. We can say that the chamber pressure will be a major drive for regression rate as the O/F is highly depends on the mean oxidizer mass flux.

Besides that, we can also study the time evolution of the chamber pressure by assuming that the nozzle throat immediately chokes where there will be a balance between the gases coming into the solid fuel and gases leaving the nozzle choked are by:

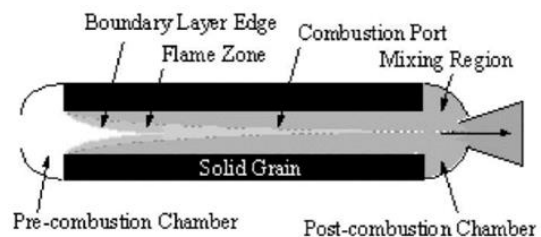


Figure 2 Longitudinal boundary layer development within the fuel port [27]

1.2 The Nozzle Theory

A nozzle is one of the most important part or section in any rocket. It functions by choking the gas flow from the combustion chamber before it goes to the atmospheric pressure surroundings. This choking action forces the gas to flow faster and thus creating low pressure region according to Bernoulli's Principle. As we all know, fluid flow from a high-pressure region to a lower region and this activity increase the speed of gas flowing thus creating thrust at the nozzle exit where the gas expands to atmospheric pressure.

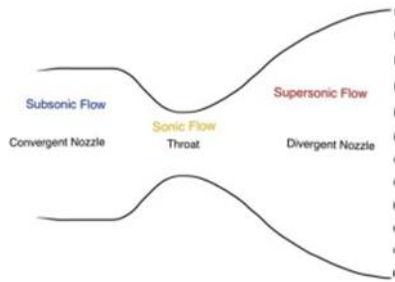


Figure 3 A nozzle diagram [27]

There are several types of nozzle configurations and the most old and common ones is the cone nozzle where the further improved version of it is called the bell-shaped nozzle. Nozzles usually have a converging and diverging section plus a throat between them, Figure 3. A converging section is not a critical part in nozzle when compared to throat and diverging section. The flow in converging section is in subsonic and the converging angle can be in any value as it can turned down a pressure easily. A few small attitude control thrust chambers have had their nozzle at 90 degrees from the combustion chamber axis without any performance loss [31]. The throat can also be in any radius as it will be acceptable. The main part, which differentiates configuration nozzles, would be the diverging section where the supersonic flow took place. A nozzle should be avoided from any sharp edges, rough surfaces and gaps in order to create a smooth flow for gaseous by minimizing skin friction.

In this study we are applying the concept of an ideal rocket in order to express its thermodynamic principles in mathematical relationships. Conservation of mass principle can be expressed by equating the mass flow rate at x to y. In mathematical form, it is known as the continuity equation and can be written in terms of cross-sectional area A, velocity v, and specific volume V.

$$\dot{m}_x = \dot{m}_y = \dot{m} = Av/V \quad (13)$$

We should then assume that an ideal rocket involved with working substance that obeys the perfect gas law. The perfect gas law is written as:

$$p_x V_x = RT_x \quad (14)$$

Where R is the gas constant to be in the value of $R=345.7 \text{ J/kg.K}$. For an isentropic flow, the temperature relations are as follows:

$$T_x/T_y = (P_x/P_y)^{(k-1)/k} = (V_y/V_x)^{k-1} \quad (15)$$

The local temperature and pressure will reach near to stagnation pressure and temperature when a local velocity approaching zero. For the case in a combustion chamber, the local combustion pressure will equal to stagnation pressure. The speed of sound in ideal gas is not depending on pressure. The formula for it is:

$$a = \sqrt{kRT} \quad (16)$$

A Mach Number, M is used to show the ratio between the flow velocity v, to the local acoustic velocity a. It is:

$$M = \frac{v}{\sqrt{kRT}} \quad (17)$$

A nozzle exit velocity for a constant k and the chamber section is larger than the nozzle throat can be determine by the following formula:

$$v_2 = \sqrt{\frac{2kRT_1}{k-1} \left[1 - \left(\frac{P_2}{P_1} \right)^{\frac{(k-1)}{k}} \right]} \quad (18)$$

From the equation above, we can see that the nozzle exit velocity is a function of pressure ratio P_1/P_2 , ratio of specific heats k, and the absolute temperature at the nozzle inlet T_1 .

The relations between the smallest nozzle area which is the throat area to the nozzle exit area is called the nozzle expansion ratio ϵ .

$$\epsilon = \frac{A_{exit}}{A_t} \quad (19)$$

We can find the thrust of a nozzle by using the following formula:

$$F = C_F A_t P_1 \quad (20)$$

Thrust coefficient C_F can be determined by experimentally from measured values of chamber pressure, throat diameter and thrust. All of the values obtained can be used in the formula:

$$C_F = \frac{v_2^2 A_2}{P_1 A_t V_2} + \frac{P_2 A_2}{P_1 A_t} - \frac{P_3 A_2}{P_1 A_t} \quad (21)$$

We can then find characteristic velocity c^* , which is the function of propellant characteristics and combustion chamber design by the following:

$$c^* = \frac{P_1 A_t}{\dot{m}} \quad (22)$$

The chemical equilibrium formula for the combustion process of stearic acid ($C_{18}H_{36}O_2$) and aluminum Al with nitrous oxide (NO_2). The combustion process of stearic acid ($C_{18}H_{36}O_2$) with aluminum (Al) and nitrous oxide



This equation represents the combustion of stearic acid ($C_{18}H_{36}O_2$) with aluminum (Al) and nitrous oxide (NO_2), resulting in the formation of carbon dioxide (CO_2), water (H_2O), aluminum oxide (Al_2O_3), and nitrogen gas (N_2).

II. SETUP AND METHODOLOGY

2.1 Test Facility

Figure 4 shows the static test stand used for the hybrid rocket engine in this study. As can be seen, the combustion chamber is made of a 460 mm-long aluminum cylindrical chamber with inner diameter of 64 mm. This chamber has a steel-made convergent-divergent nozzle that is fitted into aluminum block with throat diameter of 10 mm and length of 62.6 mm at one end, and aluminum-made axial injector at its other end. The convergent and divergent angles of the nozzle are 45° and 15° , respectively.

The fuel grain underwent independent treatment prior to being cast inside the combustion chamber and ignited. The creation and installation of a unique feed line makes it simpler to supply both gaseous oxygen and nitrous oxide. The principal oxidizer feed line has been constructed using a stainless steel pipe tubing with outside diameter of 6.35 mm and interior diameter of 3 mm. This line is fitted with a variety of valves, regulators and also pressure gauges to ensure a complete control of oxidizer flow at the required injection pressure.



Figure 4 Static test stand for hybrid rocket engine

2.2 Fuel Grain Processing

For this study, stearic acid doped with aluminum (Al) and carbon nanotubes (CNT) served as the fuel. To create the fuel grains, the wax is first heated and then casted into the proper mold. One kilogram of the required quantity is added to a stainless steel beaker. After that, the wax in this beaker is gently warmed inside the water bath while being regularly agitated. This is done until all the wax has melted and made a homogenous liquid. A revolving stirrer made of stainless steel is used to properly blend and homogenize the liquid wax after it is mixed with 3% CNT and 27% Al

(NO_2) involves several chemical reactions. However, the balanced chemical equation for the overall combustion process can be represented as follows:

powder by weight. Subsequently, the liquid wax mixture is carefully poured into the mold until it had the right size and shape. It is discovered that the liquid wax combination had a propensity to cool unevenly, leaving cavities inside the fuel grain. To address this issue, random injections of more liquid wax into the mold are made. The mold is left alone for two hours to cool to room temperature. The fuel grains are then meticulously taken out of the mold by hand, examined for cracks and then stored in a polythene bag to prevent contamination. The prepared stearic acid wax fuel grain is depicted in Figure 5.



Figure 5 Fuel grain for the hybrid rocket engine

2.3 Radio Frequency Control Unit

Meanwhile, a portable control unit has been designed to remotely manage the operation of all valves and motor ignition. This unit is powered by a rechargeable 12-volt Li-PO battery, ensuring its versatility for both laboratory and field applications, especially when the oxidizer tank has to be filled on-site before lift-off. The remote control of the valves also serves as the fail-safe mechanism in case of a power outage, enabling the system to be depressurized.

Figure 6 and Figure 7 show the constructed portable control unit. The control box is equipped with two separate arming circuits: one for the filling process and another for motor ignition. The LED indicator will be activated when the firing system is armed, serving as a warning signal to all personnel involved and highlighting potential hazards. This precaution is necessary due to distinct control circuit for the valve actuator. A modified H-bridge configuration allows for remote control of the valve circuit to utilize a

separate power source, preventing the need to transmit the high currents through the building's sensor wiring, which is not advisable.



Figure 6 Radio frequency test unit



Figure 7 Radio frequency receiver unit

2.4 Oxidizer Tank

The mass ratio of the engine is crucially affected by the oxidizer tank in a hybrid rocket system. Depending on whether the hybrid motor is turbo pump-fed or pressure-fed, the structural weight of the oxidizer tank can change dramatically. At the moment, the industry's top option is the turbo pump feed system. Nonetheless, the pressurized propellant tanks are also now practicable for use in flight applications due to progress in composite technology.

A basic oxidizer tank configuration typically consists of a cylindrical body enclosed by end caps. The cylinder bears the entirety of the hoop loading while the end caps serve to seal the ends of the cylinder. In the meantime, the structural rods handle the longitudinal loads. Propellants are kept separate from the oxidizer and fuel tanks in hybrid propellant rocket engine configuration. The oxidizer tank has fill openings for nitrous oxide and a load cell has been mounted on top of the tank. A nitrous oxide fill bottle is safely connected to the tripod beam structure next to the oxidizer tank such that it may provide nitrous oxide to the tank through aluminum pressure pipe. The pressure relief

valve in the nitrous oxide fill system has a larger capacity than the regulator and is set to a relief pressure lower than any system component's rated pressure. Additionally, the regulator is used at the nitrous oxide supply bottle to lower the tank's pressure to the required amount. The pressures for the tank and the supply are measured by two gauges. A valve is fitted on oxidizer tank's upper bulkhead to make it possible to turn off the nitrous oxide supply as necessary.

Figure 8 shows the test rig for the oxidizer system that is used in this study.



Figure 8 Oxidizer system test rig

2.5 Injector Manifold

The crucial mixing process occurs inside the injector, which is positioned directly above the primary combustion chamber. It performs a function that is closely similar to a carburetor in an internal combustion engine. One of the injector's key responsibilities is to introduce and precisely control the flow of liquid propellants into the combustion chamber, which causes the liquids to atomize and separate into tiny droplets. Additionally, the injector is in charge of evenly dispersing and thoroughly blending the propellants, ensuring the production of appropriately balanced mixture of fuel and oxidizer. Through this process, the propellant mass flow and also composition are kept constant across the chamber's cross-section.

To determine the necessary orifice diameter for the injector, a specific method is employed, as outlined. This approach applies to subsonic flows through the orifice and assumes that the flow is essentially incompressible. The mass flow rate through the injector is given by Equation (24), where A_2 is the injector orifice area, and ρ_2 and u_2 are the gas density and velocity at the injector exit, respectively. In the meantime, μ is the flow coefficient or ratio of actual to ideal mass flow rate, which for an incompressible fluid is expressed in Equation (25), where ζ_i is the hydraulic loss coefficient of the injector that can be computed by using Equation (26). In Equation (26) d_i is the orifice diameter, d_l is the diameter of the gas flow upstream of the orifice and l_i is the length of the orifice. λ is the drag coefficient of the injector passage, expressed

for hydraulically smooth pipes while ξ_{in} is hydraulic loss coefficient of the injector inlet and is a function of the inlet geometry. For a sharp-edged conical inlet, it is a function of the convergence angle and the ratio of convergent length to orifice diameter.

$$\dot{m}_i = \mu \rho_2 u_2 A_2 \quad (24)$$

$$\mu = \frac{1}{1 + \xi_i} \quad (25)$$

$$\xi_i = \xi_{in} \left(1 - \frac{d_i^2}{d_1^2} \right) + \lambda \frac{l_i}{d_i} \quad (26)$$

Based on the geometry of off-the-shelf orifices used in the present work and assuming isentropic flow through the orifice, the gas density at the exit may be obtained from Equation (27). Furthermore, the ideal exit velocity u_2 can be expressed as shown in Equation (28). In these equations, p_{01} is the total pressure of the flow, p_c is the sum of chamber pressure and injector pressure drop, and total temperature T_{01} is the gas temperature upstream of the injector in the manifold.

$$\rho_2 = \rho_{01} \left(\frac{p_2}{p_{01}} \right)^{1/\gamma} \quad (27)$$

$$u_2 = \sqrt{2 \frac{\gamma}{\gamma - 1} RT_{01} \left[1 - \left(\frac{p_c}{p_{01}} \right)^{\frac{\gamma}{\gamma - 1}} \right]} \quad (28)$$

For a given injector inlet pressure, the exit velocity reaches its theoretical maximum limit of $p_c = 0$. Hence, the velocity coefficient λ_2 is defined in Equation (29), which is then allows Equation (24) to be expressed as Equation (30). In this equation, c^* is the characteristic velocity as defined in Equation (31). Moreover, the gas-dynamic function can also be written as Equation (32).

$$\lambda_2 = \frac{u_2}{u_{th}} = \sqrt{\frac{\gamma + 1}{\gamma - 1} \left[1 - \left(\frac{p_c}{p_{01}} \right)^{\frac{\gamma}{\gamma - 1}} \right]} \quad (29)$$

$$\dot{m}_i = \mu \frac{(p_2 + \Delta p_i) A_n}{c^*} q(\lambda_2) \quad (30)$$

$$c^* = \frac{\sqrt{\gamma RT_{01}}}{\gamma \sqrt{\left(\frac{2}{\gamma - 1} \right)^{\frac{\gamma + 1}{\gamma - 1}}}} \quad (31)$$

$$q(\lambda_2) = \lambda_2 \left(\frac{\gamma + 1}{2} \right)^{\frac{1}{\gamma - 1}} \left(1 - \frac{\gamma - 1}{\gamma + 1} \lambda_2^2 \right)^{\frac{1}{\gamma - 1}} \quad (32)$$

For this study, the final orifice diameter predicted by this procedure is 1 mm. An additional choke hole is added to the nitrous oxide feed line upstream of the injector to ensure consistent mass flow rate and complete decoupling of the feed system from combustion chamber. An upstream

pressure of at least 203 psi (14 Bar) is necessary to ensure that this orifice stays choked over the whole range of the expected chamber pressure. Figure 9 and Figure 10 display the bulkhead with oxidizer injector and the conducted test of the injector, respectively.



Figure 9 Bulkhead with oxidizer injector



Figure 10 Oxidizer injector test

III. RESULTS AND DISCUSSION

3.1 Estimated rocket motor and nozzle sizing

Information regarding characteristic velocity and specific heat ratio for propellants is collected using NASA's chemical equilibrium software CEA. This collection assumes a stagnant flow within the combustion chamber [40].

Initial Parameters:

$$P_2/P_3 = 0.1013$$

$$P_c/P_1 = 1.2$$

$$k = 1.308$$

$$T_1 = 2500 \text{ K}$$

$$P_x = 0.5 \text{ MPa}$$

$$R = 345.7 \text{ J/kg.K}$$

$$F = 300 \text{ N}$$

Thrust, from Equation (20), $F = C_F P_C A_t$, $300 = (1.5)(1.2 \times 10^6)A_t$, $A_t = 1.667 \times 10^{-4} \text{ m}^2$.

Mass flow rate, from Equation (22), $\dot{m} = \frac{P_C A_t}{C^*}$, $\dot{m} = \frac{(1.2 \times 10^6)(1.667 \times 10^6)}{1197.84} = 0.167 \text{ kg/s}$.

Initial specific volume, from Equation (14), $V_1 = \frac{RT_1}{P_1}$, $V_1 = \frac{(345.7)(2500)}{1.2 \times 10^6} = 0.72 \text{ m}^3/\text{kg}$.

Specific volume, from Equation (14), $V_x = V_1 \left(\frac{P_1}{P_x}\right)^{\frac{1}{k}}$, $V_x = 0.72 \left(\frac{1.2 \times 10^6}{0.5 \times 10^6}\right)^{\frac{1}{1.308}} = 1.406 \text{ m}^3/\text{kg}$.

Specific Temperature, from Equation (15), $T_x = T_1 \left(\frac{P_x}{P_1}\right)^{\frac{(k-1)}{k}}$, $T_x = 2500 \left(\frac{0.5 \times 10^6}{1.2 \times 10^6}\right)^{\frac{(1.308-1)}{1.308}} = 2034.28 \text{ K}$.

Specific velocity, from Equation (18), $v_x = \sqrt{\frac{2kRT}{k-1} \left[1 - \left(\frac{P_x}{P_1}\right)^{\frac{(k-1)}{k}}\right]}$, $v_x = \sqrt{\frac{2(1.308)(345.7)(2500)}{(1.308-1)} \left[1 - \left(\frac{0.5 \times 10^6}{1.2 \times 10^6}\right)^{\frac{(1.308-1)}{1.308}}\right]} = 1169.38 \text{ m/s}$.

Specific area, from Equation (13), $A_x = \frac{\dot{m}_x V_x}{v_x}$, $A_x = \frac{(0.167)(1.406)}{1169.38} = 2.008 \times 10^{-4} \text{ m}^2$.

Specific Mach number, from Equation (17), $M_x = \frac{v_x}{\sqrt{kRT_x}}$, $M_x = \frac{1169.38}{\sqrt{(1.308)(345.7)(2034.28)}} = 22$

* at optimum expansion, ideal exhaust velocity is $c = v_2$,

from Equation (18), $v_2 = \sqrt{\frac{2kRT}{k-1} \left[1 - \left(\frac{P_2}{P_1}\right)^{\frac{(k-1)}{k}}\right]}$, $v_2 =$

$$\sqrt{\frac{2(1.308)(345.7)(2500)}{(1.308-1)} \left[1 - \left(\frac{0.1013 \times 10^6}{1.2 \times 10^6}\right)^{\frac{(1.308-1)}{1.308}}\right]} = 1799.76 \text{ m/s}$$

Thrust, $F = \dot{m} v_2$, $F = (0.167)(1799.76) = 300.56 \text{ N}$.

Specific Impulse, from Equation (22), $I_s = \frac{c}{g_0}$, $I_s = \frac{1799.76}{9.81} = 183.46 \text{ s}$.

Specific volume at exit, from Equation (15), $V_2 = V_1 \left(\frac{P_1}{P_2}\right)^{\frac{1}{k}}$, $V_2 = 0.72 \left(\frac{1.2 \times 10^6}{0.1013 \times 10^6}\right)^{\frac{1}{1.308}} = 4.765 \text{ m}^3/\text{kg}$.

Area at nozzle exit, from Equation (13), $A_2 = \frac{\dot{m} V_2}{v_2}$, $A_2 = \frac{(0.167)(4.765)}{1799.76} = 4.421 \times 10^{-4} \text{ m}^2$

Nozzle expansion ratio, from Equation (19), $\epsilon = \frac{A_{exit}}{A_t}$, $\epsilon = \frac{4.421 \times 10^{-4}}{1.667 \times 10^{-4}} = 2.65$

Exit temperature, from Equation (15), $T_2 = T_1 \left(\frac{P_2}{P_1}\right)^{\frac{(k-1)}{k}}$, $T_2 = 2500 \left(\frac{0.1013 \times 10^6}{1.2 \times 10^6}\right)^{\frac{(1.308-1)}{1.308}} = 1396.82 \text{ K}$

* by assuming initial mixture ratio, O/F = 1, $\dot{m} = \dot{m}_f + \dot{m}_o$, $\dot{m}_f, \dot{m}_o = \frac{0.167}{2} = 0.0835 \text{ kg/s}$

Mass flow rate of fuel, \dot{m}_f (value for \dot{r} was taken to be 0.0015 m/s from past research of paraffin wax [33], value for ρ_f was taken to be 862 kg/m³ for stearic acid [34], from Equation (10), $\dot{m}_f = \rho_f \dot{r} A_b$, $0.0835 = 862(0.0015)A_b$, $A_b = 0.0646 \text{ m}^2$, where A_b is burn area of fuel, Chamber length, $L_c = 0.2773 \text{ m}$, Chamber diameter, $2\pi r_c L = A_b$, $r_c = \frac{0.0646}{2\pi(0.2773)} = 0.03708 \text{ m}$, $D_c = 0.3708 \text{ m} \times 2 = 0.0742 \text{ m}$

Throat diameter, $A_t = \pi r_{throat}^2$, $r_t =$
 $\sqrt{\frac{1.667 \times 10^{-4}}{\pi}} = 7.284 \times 10^{-3} \text{ m}$, $D_t = 7.284 \times$
 $10^{-3} \text{ m} \times 2 = 0.0146 \text{ m}$

Nozzle exit diameter, $A_2 = \pi r_{exit}^2$, $r_e =$
 $\sqrt{\frac{4.421 \times 10^{-4}}{\pi}} = 0.0119 \text{ m}$, $D_e = 0.0119 \text{ m} \times 2 =$
 0.0238 m

Nozzle converging section, converging angle, $\beta =$
 45° , Chamber to nozzle length, $a = \frac{(D_c - D_t)/2}{\tan 45^\circ}$, $a =$
 $\frac{(0.0742 - 0.0146)/2}{\tan 45^\circ} = 0.0298 \text{ m}$

Nozzle diverging section, diverging angle, $\alpha = 12^\circ$,
 Throat to nozzle exit length, $b = \frac{(D_e - D_t)/2}{\tan 12^\circ}$, $b =$
 $\frac{(0.0238 - 0.0146)/2}{\tan 12^\circ} = 0.0433 \text{ m}$

3.2 Motor Tests and Post-Analyses

Hot-fire testing of the constructed lab-scale design of the green hybrid rocket motor has been successfully done as shown in Figure 11.

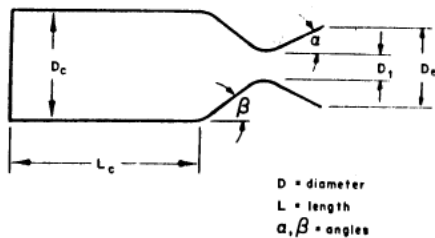


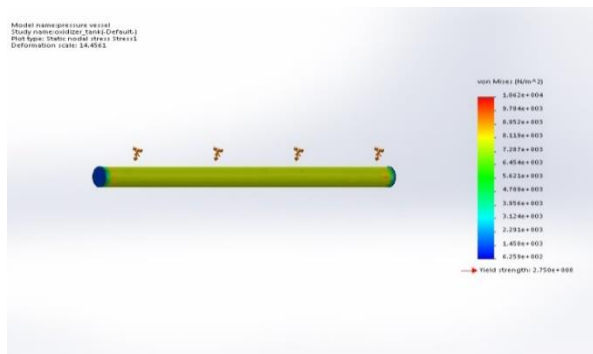
Figure 11 A nozzle configuration [35]

All systems that are designed and developed for the hybrid rocket engine have been shown to be successful, including the radio frequency control unit. Data from the experiment has been gathered using Arduino system. It should be noted that prior to the hot-fire test, the standard cold-flow tests have been carried out to validate the control system, check the ignition firing sequence and establish requirements for the feed line pressure drop and oxidizer flow rate.

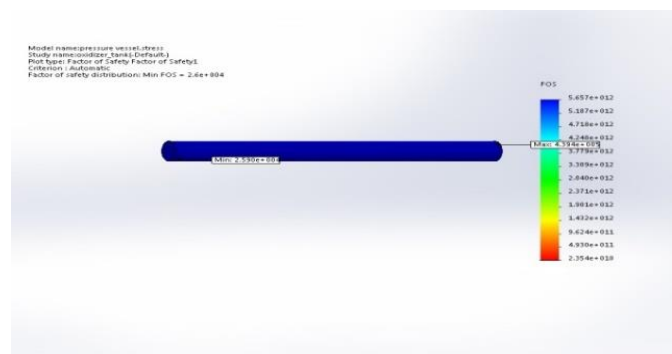
3.2 Simulation Analysis on Bulkhead and Oxidizer Tank

The objective of this analysis is to examine potential deformation in the rocket motor's component elements and determine whether the structure can withstand the pressure and heat. To perform this study, SolidWorks Simulation is used, which is a design analysis tool that is fully integrated with SolidWorks. Specifically, the analysis uses the finite element method (FEM) capability of the software, which is one of the widely-used computational techniques for the evaluation of engineering design. Among others, FEM has been applied through simulation in various studies such as for structural analysis of aircraft wing box [37], flapping wing mechanism [38] and also aircraft passenger seat [39]. In this study, the focus is on the static study, which is also often referred to as stress studies. Static studies are used to calculate displacements, reaction forces, strains, stresses and the distribution of the safety factor.

It should be noted that the stress distribution chart uses colors to indicate the stress level, with blue signifying lower stress and red denoting higher stress. The results of the simulation analysis, which are depicted in Figure 12 and Figure 13, show that the greatest stress does not exceed the ultimate tensile strength of the material used for the tanks and their bulkheads. It is encouraging to see that the stress distribution is still within a safe range. The final design of the green hybrid rocket engine for this study is decided and finalized based on the simulation finding. The final design specifications are tabulated in Table 1.

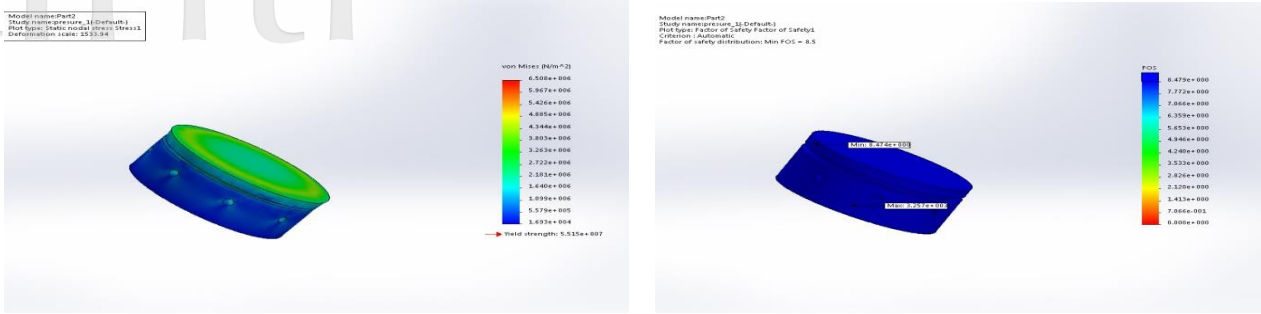


(a) Initial pressure tank



(b) Oxidizer tank

Figure 12 Stress analysis results for the tanks



(a) Initial pressure tank bulkhead

(b) Oxidizer bulkhead

Figure 13 Stress analysis results for the bulkheads

Table 1 Design specifications of the green hybrid rocket engine

Initial Tank: Supercharge Gas Initial Tank Pressure [psi]	Nitrogen 754
Oxidizer Tank: Oxidizer Loaded Oxidizer Mass [kg] Oxidizer Flow Rate [kg/s]	Nitrous Oxide 0.65 0.01
Combustion Chamber Chamber Pressure [psi] Temperature [°C] Oxidizer-to-Fuel Ratio	203 185 8.034
Propellant Composition Grain Configuration Number of Ports Initial Port Diameter [mm] Grain Length [mm] Grain Diameter [mm] Fuel Mass [kg]	70 % SA Wax, 27 % AL, 3 % CNT Cylindrical 1 15 370 65 1.43
Nozzle Material Shape Expansion Ratio Throat Diameter [mm] Exit Diameter [mm] Thrust [N]	Aluminium Conical Nozzle 3.88 15 44 348

of thrust versus time. The plots highlight on how a hybrid rocket motor with a blowdown motor system operates. In short, the observation has demonstrated the occurrence of a brief peak immediately following the igniter burnout, which is followed by development of a stable combustion condition. The peak thrust is potentially decreased due to the decreased oxidizer mass flow rate and also combustion efficiency. Figure 15 illustrates the progressive buildup of the chamber pressure, eventually reaching a steady state. During this steady-state phase, the mean pressure has been recorded at 203 psi, with pressure oscillations fluctuating within a range of ± 3 psi from the mean value. Meanwhile, the thrust profile during the firing is observed in Figure 16, which reveals a maximum thrust of 348 N. It can be seen that the thrust initially increases, then begins to stabilize, mirroring the trends seen in the pressure-time history. Last but not least, Figure 17 shows the plot of the temperature of the chamber versus time. From this plot, it can be seen that the average combustion temperature is 140°C, which is double the melting of stearic acid (i.e. 69°C – 70°C).



Figure 14 Hybrid rocket test

The effective firing of the green hybrid rocket engine is done close to UPM. The motor intended for the rocket static testing is used in the experiment as shown in Figure 14. It can be noted that the igniting procedure has produced a maximum combustion chamber pressure of 14 bar and a peak thrust of 348 N. Moreover, Figure 15 and Figure 16 respectively show the plot of pressure against time and that

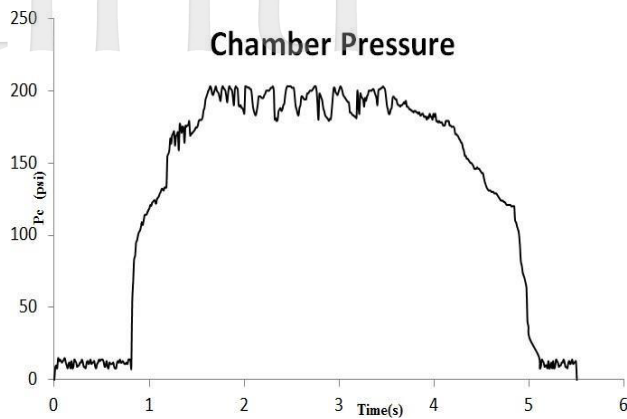


Figure 15 Chamber pressure versus time [18]

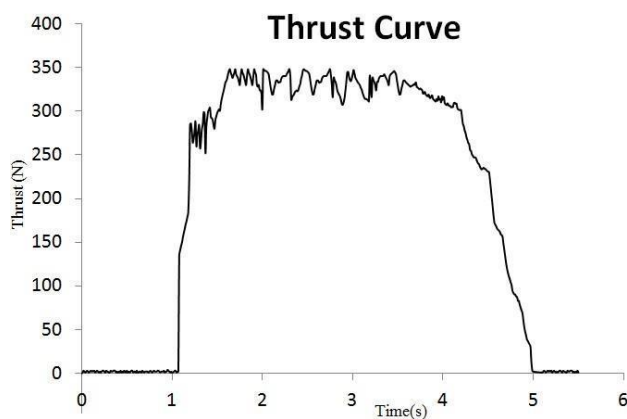


Figure 16 Produced thrust versus time [18]

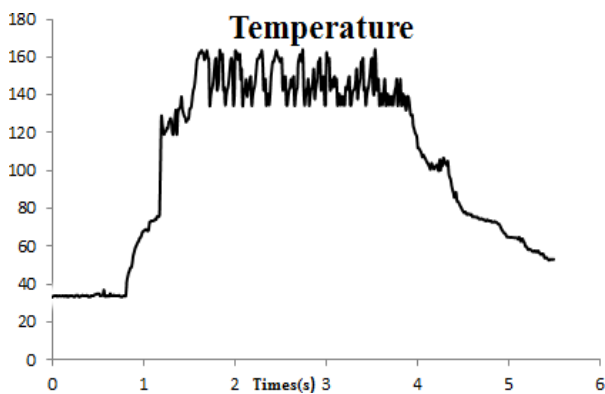


Figure 17 Chamber temperature versus time [18]

IV. CONCLUSIONS

The laboratory-scale green hybrid rocket motor's hot-fire experiments have been successfully conducted and the obtained results have provided an insightful information on how well it performed. The motor has been successfully ignited and produced a maximum thrust of 348 N, with the maximum combustion chamber pressure is recorded as 14

bar. The pressure and thrust profiles show that the motor used a blowdown propulsion system. The motor's output peaked briefly after igniter burnout and then continued to burn steadily after that. However, it is noteworthy to note that steady-state combustion was accompanied by pressure oscillations within a range of ± 3 psi from the mean value, which might require further investigation to optimize the combustion stability.

Several recommendations can also be made based on the findings of this study and they are listed as follow:

- Improve combustion stability: Take necessary steps to reduce the pressure oscillations that have been noticed during steady-state combustion. Possible changes that can be made is to use the conditions for the optimum combustion efficiency and fine-tuning the mass flow rate of the oxidizer.
- Extensive data analysis: To have deep understanding of the operation of the motor, a thorough study can be conducted using the gathered data. The assessment of the connection between thrust and chamber pressure, as well as the effects of various parameters on motor performance, should be included in this analysis.
- Material and component evaluation: Keep checking to see if the materials and parts used to build the motor are appropriate. This ongoing evaluation is intended to improve overall dependability and efficiency.
- Extended testing regimen: Take into account running additional tests to improve the performance and also design of the motor. Each test iteration should guide small tweaks, enabling ongoing improvement based on the knowledge learned from earlier testing.

By addressing these recommendations and building upon the insights gained from this testing phase, the work will aid in enhancing the overall performance and reliability of the hybrid rocket motor for future applications.

ACKNOWLEDGMENTS

The authors like to thank Prof. Dr. Azizi Miskon of National Defence University of Malaysia and his working group for their funding and support for our research on the hybrid rocket design and development.

REFERENCES

- [1] Venugopal S, Rajesh KK, Ramanujachari V, "Hybrid rocket technology," *Defence Science Journal*, Vol. 61, No. 3, 2011.
- [2] Chang MF, Hsing YC, "The performance of hybrid rocket with various oxidizers," *Journal of Aeronautics, Astronautics and Aviation*, Vol. 40, No. 1, 2008, pp. 35-40.
- [3] Hikone S, Maruyama S, Isiguro T, Nakagawa I, "Regression rate characteristics and burning mechanism of some hybrid rocket fuels," *Proceedings of 46th AIAA/ASME/SAE/ASEE Joint Propulsion Conference & Exhibit*, 2010.

- [4] Oztan C, Coverstone V, "Utilization of additive manufacturing in hybrid rocket technology: A review," *Acta Astronautica*, Vol. 180, 2021, pp. 130-140.
- [5] Sabri MEE, Azami MH, Abdullah NA, Nordin NH, "Investigation of regression rate end-burning typed hybrid rocket motor," *Journal of Aeronautics, Astronautics and Aviation*, Vol. 55, No. 3S, 2023, pp. 485-494.
- [6] Rabinovitch B, "Regression rates and the kinetics of polymer degradation," *Proceedings of International Symposium on Combustion*, 1965.
- [7] Houser TJ, Peck MV, "Research in hybrid combustion," *Progress in Astronautics and Rocketry*, Vol. 15, 1964, pp. 559-581.
- [8] Green Jr L, "Introductory considerations on hybrid rocket combustion," *Progress in Astronautics and Rocketry*, Vol. 15, 1964, pp. 451-484.
- [9] Marxman G, Gilbert M, "Turbulent boundary layer combustion in the hybrid rocket," *Proceedings of the International Symposium on Combustion*, 1963.
- [10] Marxman GA, "Combustion in the turbulent boundary layer on a vaporizing surface," *Proceeding of International Symposium on Combustion*, 1965.
- [11] Marxman GA, Woolridge CE, "Research on the combustion mechanism of hybrid rockets," *Proceedings of AGARD Colloquium on Progress in Tactical Rocket Propulsion*, 1968.
- [12] Marquardt T, Majdalani J, "A primer on classical regression rate modeling in hybrid rockets," *Proceedings of AIAA Propulsion and Energy Forum*, 2020.
- [13] Zakirov V, Sweeting M, Lawrence T, Sellers J, "Nitrous oxide as a rocket propellant," *Acta Astronautica*, Vol. 48, 2001, pp. 353-362.
- [14] Karabeyoglu MA, "Nitrous oxide and oxygen mixtures (Nytrox) as oxidizers for rocket propulsion applications," *Journal of Propulsion and Power*, Vol. 30, No. 3, 2014, pp. 696-706.
- [15] Paravan C, Hashish A, Santolini V, "Test activities on hybrid rocket engines: combustion analyses and green storable oxidizers—a short review," *Aerospace*, Vol. 10, No. 7, 2023, 572.
- [16] Cantwell B, Karabeyoglu A, Altman D, "Recent advances in hybrid propulsion," *International Journal of Energetic Materials and Chemical Propulsion*, Vol. 9, No. 4, 2010.
- [17] Ahmad MT, Abidin R, Latif Taha A, Anudip, Amzaryi, "Feasibility study of palm-based fuels for hybrid rocket motor applications," *AIP Conference Proceedings*, 1930, 020010 (2018)
- [18] Ahmad MT, Jagannathan A, Abidin R, Noordin MNH, Wan Ya'acob WMH, Zhahir A, Azami MH, "Ballistic test investigation of hybrid rocket motor utilizing stearic acidbiofuel with energetic additives for regression rate enhancement," *AIP Conference Proceedings* 2339, 020174 (2021). <https://doi.org/10.1063/5.0044504>
- [19] Sutton GP, Biblarz O, "Rocket Propulsion Elements" Seventh Edition, Wiley, 2001.
- [20] Marxman G, Gilbert M, "Turbulent boundary layer combustion in the hybrid rocket," *Symposium (International) on Combustion*, Vol. 9, 1963, pp. 371-383.
- [21] Marxman G, Wooldridges C, Muzzy R, "Fundamentals of Hybrid Boundary Layer Combustion," *AIAA Heterogeneous Combustion Conference*, 1963.
- [22] Bombelli V, Simon D, Moerel TMJL, "Economic Benefits of the use of Non-Toxic Mono-Propellants for Spacecraft Applications," 39th Joint Propulsion Conference, Huntsville, Ala., July 2003.
- [23] Peterson Z, Eilers SD, Whitmore S, "Closed-Loop Thrust and Pressure Profile Throttling of a Nitrous-Oxide HPTB Hybrid Rocket Motor," *AIAA 2012-4551*, 2012.
- [24] Karabeyoglu A, Stevens J, Cantwell B, "Investigation of Feed System Coupled Low Frequency Combustion Instabilities in Hybrid Rockets," *AIAA 2007-5366*, 2007.
- [25] American Institute of Aeronautics and Astronautics, *Fundamentals of Hybrid Rocket Combustion and Propulsion*, American Institute of Aeronautics and Astronautics, Inc., 2007.
- [26] 3136119, U.S.P.N., No. 3136119, June 9, 1964.
- [27] Jonathan M. McCulley, "Design and Testing of Digitally Manufactured Paraffin Acrylonitrile-butadiene-styrene Hybrid Rocket Motors," 2012, pp. 13.
- [28] "Hybrid Rocket Engine (liquid oxidizer, solid fuel)," (Rrwillhelm Projects). Retrieved from November 2, 2015, from <http://www.rwillhelm.com/port/other/other.php>
- [29] Anthony J. Marchese, "Development and Testing of a Hybrid Rocket Motor in a Rocket Propulsion Course," 2006.
- [30] Tariq Malik, "SpaceShipOne Rocket Engine Gets an Upgrade," 2004.
- [31] George P. Sutton, Oscar Biblarz, "Rocket Propulsion Elements," Seventh Edition, 2001, pp. 75.
- [32] George P. Sutton, Oscar Biblarz, "Rocket Propulsion Elements," Seventh Edition, 2001, pp. 76.
- [33] Bernard Genevieve, Michael J. Brooks, Jean-Fraincois P. Pitot de la Beaujardiere, Lance W. Roberts, "Performance Modeling of a Paraffin Wax / Nitrous Oxide Hybrid Rocket Motor," 2011, pp. 11.
- [34] Tiong Chiong Ing, A. K. Mohammed Rafiq, Y. Azli, S. Syahrullail, "The Effect of Temperature on the Tribological Behavior of RBD Palm Stearin," 2012, pp. 540.
- [35] "Design Equations," (Risacher). Retrieved from December 15, 2015, from <https://www.risacher.org/rocket/eqns.html>
- [36] "Nozzle Flow Theory," (Hybrid Rocket Engine Project). Retrieved from December 17, 2015, from <https://hybridrocketengine.wordpress.com>
- [37] Othman MS, Chun OT, Harmin MY, Romli FI, "Aeroelastic effects of a simple rectangular wing-box model with varying rib orientations," *IOP Conference Series: Materials Science and Engineering*, Vol. 152, No. 1, 2016, 012009.

[38] Kompala S, Esakki B, Yang LJ, Wang WC, Reshmi W, Chin YJ, “Fabrication of flapping wing mechanism using fused deposition modeling and measurement of aerodynamic forces,” *Journal of Aeronautics, Astronautics and Aviation*, Vol. 51, No. 1, 2019, pp. 131-140.

[39] Mohamad Nor AR, Romli FI, “Analysis of a new standing passenger seat design for commercial transport aircraft,” *ARPJ Journal of Engineering and Applied Sciences*, Vol. 18, No. 6, 2023, pp. 640-647.

[40] Gordon S, McBride BJ, Computer program for calculation of complex chemical equilibrium compositions and applications. (1994)

Symbols used

a	Absorption coefficient
$A_{chamber}$	Regression rate using pixelated disk filter
A_{ox}	Injector discharge area
A_{port}	Port area
B	Blowing parameter
C_d	Injector discharge coefficient
C_H, C_{H0}	Stanton number with and without blowing
c_p	Specific heat
G	Instantaneous mas flux
h_v	Heat of vaporization
L	Motor length
\dot{m}_{ox}	Oxidizer mass flow rate
n	Rows of \bar{I}
P_0	Combustion pressure
P_{ox}	Oxidizer pressure
P_r	Prandtl number
\dot{Q}_w	Heat transfer to the wall
\dot{r}	Regression rate
T	Temperature
T_0	Combustion flame temperature
T_{fuel}	Fuel temperature
V_c	Fuel port volume
ΔH	Effective heat of gassification
μ	Viscosity
ρ	Density
ρ_{fuel}	Fuel density
ρ_{ox}	Oxidizer density

Nozzle Nomenclature:

D_c	Chamber Diameter
L_c	Length Chamber
L_n	Length Divergent
D_t	Diameter Throat
D_e	Diameter Exit
α	Divergent Angle
θ	Convergent Angle

Nozzle Flow Parameters:

P	Pressure (Pa)
T	Temperature (K)
V_e	Velocity (m/s)
A	Area (m ²)
C_p	Specific Heat at Constant Pressure (J/Kg K)
C_v	Specific Heat at Constant Volume (J/Kg K)
γ	Specific heat ratio (Cp/Cv)
R	Specific Gas Constant (J/Kg K)
h	Enthalpy (J/Kg K)
\dot{m}	Mass Flow Rate (Kg/s)
M	Mach number